INT. J. NUM. METH. HEAT FLUID FLOW, VOL. 4, 31–45 (1994)

A BEM ANALYSIS FOR TRANSIENT CONDUCTION-CONVECTION PROBLEMS

J. LIM, C. L. CHAN AND A. CHANDRA

Department of Aerospace and Mechanical Engineering, The University of Arizona, Tucson, AZ 85721, USA

ABSTRACT

A boundary element method (BEM) formulation for the solution of transient conduction-convection problems is developed in this paper. A time-dependent fundamental solution for moving heat source problems is utilized for this purpose. This reduces the governing parabolic partial differential equations to a boundary-only form and obviates the need for any internal discretization. Such a formulation is also expected to be stable at high Peclet numbers. Numerical examples are included to establish the validity of the approach and to demonstrate the salient features of the BEM algorithm.

KEY WORDS BEM Conduction Transient analysis Moving sources

INTRODUCTION

The BEM (boundary element method) is a powerful general-purpose method[1–4]. It is far more tolerant of aspect-ratio degradation than the FEM and can yield secondary variables as accurate as the primary ones. In the BEM, the internal equations are applied pointwise. Thus, sharp temperature gradients over the domain may be easily captured. Mukherjee and Morjaria[5] compared the efficiency and accuracy of the BEM and FEM for the Laplace equation. They found that the BEM results are more accurate than the FEM for the same level of discretization. This implies that, for the same desired level of accuracy, the BEM requires a coarser mesh. On the other hand, the FEM's accuracy is very sensitive to the internal mesh. Also, the accuracy of the BEM does not change appreciably with the number of internal sampling points.

Several researchers have investigated the conduction-convection problem by FEM[6–8].The traditional Galerkin formulation, however, produces an unstable solution. A Petrov–Galerkin approach produces a stable solution, but there are noticeable differences when compared to analytical solutions. The discrepancy also gets worse as the Peclet number increases.

The BEM has been applied to several steady-state and transient diffusion problems including the effects of moving boundaries and phase changes[9–14]. Tanaka *et al.*[15] have also obtained mixed boundary element solutions of steady-state convection-diffusion problems in three dimensions using the moving heat source Jaeger solution as the fundamental solution. They found the accuracy of the BEM solutions, compared to exact solutions, to be almost independent of the Peclet number. The BEM solutions were also unconditionally stable in space. These features make the BEM superior to domain-type numerical techniques, which have a criterion for numerical stability and whose accuracy depends to some extent on the Peclet numbers.

Recently[16–19], the thermal aspects and their sensitivities in steady-state machining processes, using a BEM formulation based on the fundamental solution of the convection-diffusion operator, were investigated. Their analyses showed no indication of false diffusion. The BEM, by virtue

0961–5539/94/010031–15$2.00

Received June 1992
Revised August 1993

of its ability to determine boundary quantities accurately and internal quantities pointwise, has proved very effective in capturing the sharp temperature gradients in various steady-state machining processes.

The boundary element method has also been applied to transient convection-diffusion problems by various researchers. Curran *et al.*[20] used a time-dependent fundamental solution defined only for the diffusive terms. This requires a domain-type solution strategy. Aral and Tang[14] use a secondary reduction BEM (SR-BEM) algorithm to reduce the BEM finite difference computations for parabolic partial differential equations to a boundary-only form. Their algorithm uses the fundamental solution for the steady-state diffusion operator and requires internal discretization. The SR-BEM algorithm described by Aral and Tang is essentially a procedure for eliminating the internal degrees of freedom efficiently. Accordingly, the temporal features of a transient problem and its associated time integration schemes are not addressed. Typically, very small time steps are needed when a transient problem is attempted by employing a steady-state fundamental solution[2]. Moreover, such an algorithm is susceptible to inherent numerical oscillations and false diffusion. In view of these, a transient BEM formulation based on the time-dependent fundamental solution of the transient convection-diffusion operator is developed in the present work. This reduces the governing parabolic partial differential equation to a boundary-only form. This paper begins with a presentation of the proposed BEM formulation for transient convection-diffusion problems. A description of the numerical implementation for planar problems follows. Numerical examples are included to demonstrate the salient features of the BEM algorithm and to establish the validity of the proposed technique.

BOUNDARY ELEMENT FORMULATION

The governing equation for the transient conduction-convection problem may be expressed as:

$$\left(\frac{\partial T(\mathbf{x}, t)}{\partial t} + v_i \frac{\partial T(\mathbf{x}, t)}{\partial x_i}\right) - \kappa \frac{\partial^2 T(\mathbf{x}, t)}{\partial x_i^2} = 0 \quad \text{in } \Omega \tag{1}$$

Here, v_i is the convective velocity and $\kappa = k/\rho c$ is the thermal diffusivity. It is assumed that thermal conductivity, specific heat, and density remain constant. For situations involving spatial variations of κ, the domain B may be divided into several zones and the thermal diffusivity κ may be assumed to be piecewise constant over each of these zones. A BEM formulation for planar problems is presented in this section. A similar technique may also be used to obtain a three-dimensional BEM formulation.

In the present applications, the convective velocity is assumed to be constant in time and space. A boundary-only form of the BEM formulation is developed first. Cases involving spatially nonuniform convection velocities may also be analyzed by using zoning, such that the velocity is constant in each zone, or by introducing a domain integral incorporating the velocity gradients. The zoning approach has been used previously[17,18] for steady-state machining processes.

For constant velocities of convection, we may introduce a coordinate system with its axes oriented in parallel and normal directions to the velocity vector. Without any loss of generality, the governing equation may be expressed as:

$$\frac{\partial T(\mathbf{x}, t)}{\partial t} + \mathrm{Pe} \frac{\partial T(\mathbf{x}, t)}{\partial x_1} = \nabla^2 T(\mathbf{x}, t) \quad \text{in } \Omega \tag{2}$$

where the x_1 direction is along the direction of the resultant convection velocity. Pe is the Peclet number ($\mathrm{Pe} = VL/\kappa$). Here, V is the convective velocity in the x_1 direction, and L is a characteristic length. The boundary conditions are:

$$T(\mathbf{x}, t) = \bar{T}(\mathbf{x}, t) \quad \text{on } \Gamma_T \tag{3}$$

and

$$\frac{\partial T(\mathbf{x}, t)}{\partial x_i} n_i = \bar{q}(\mathbf{x}, t) \quad \text{on } \Gamma_q \tag{4}$$

Equation (2) applies to an Eulerian reference frame that remains spatially fixed while the material flows through it. The convective term represents the energy transported by the material as it moves through the reference frame. The surface flux $\bar{q}$ includes a contribution from convective cooling losses, $q^{(c)}$, which may be written as:

$$q^{(c)}(\mathbf{x}, t) = \mathrm{Nu}[T(\mathbf{x}, t) - T_\infty] \tag{5}$$

T_∞ represents the ambient temperature and Nu is the Nusselt number (hL/k), where h is the convective heat transfer coefficient.

Let us also consider the adjoint equation:

$$-\frac{\partial G(\mathbf{x}, t)}{\partial t} - \mathrm{Pe}\frac{\partial G(\mathbf{x}, t)}{\partial x_i} = \nabla^2 G(\mathbf{x}, t) + \delta(\mathbf{x}(q) - \mathbf{x}(p))\delta(t - \tau) \tag{6}$$

where p and q are a source point and field point, respectively, in the domain (P and Q represent a source point and field point, respectively, on the boundary), τ is the final time, and t is the time variable.

Applying the divergence theorem, and following previous procedures[15,17,18], an integral representation of the governing equation may be obtained as:

$$T(p, \tau; Q, t) = \int_0^\tau \mathrm{d}t \int_{\Gamma(t)} \left[G(p, \tau; Q, t) \frac{\partial T}{\partial n_Q}(Q, t) - \frac{\partial G}{\partial n_Q}(p, \tau; Q, t) T(Q, t) \right] \mathrm{d}\Gamma$$
$$- \mathrm{Pe} \int_0^\tau \mathrm{d}t \int_{\Gamma(t)} G(p, \tau; Q, t) T(Q, t) n_1(Q, t)\, \mathrm{d}\Gamma \tag{7}$$

The normal flux at the boundary $q(Q, t)$ is equal to $\partial T/\partial n_Q(Q, t)$. In deriving (7), it is assumed that:

$$T(\mathbf{x}, 0) = 0 \tag{8}$$

Thus, $T(\mathbf{x}, t)$ represents the temperature rise from a uniform initial temperature in the body. A domain integral appears in (7) if the initial temperature distribution is not uniform[11]. However, in many practical problems, the initial temperature distribution remains uniform and, for simplicity, this is assumed here.

The fundamental solution $G(p, \tau; q, t)$[21] is given as:

$$G(p, \tau; q, t) = \frac{1}{4\pi(\tau - t)} \exp\left[\frac{-[\{(x_1(q) - x_1(p)) + \mathrm{Pe}(\tau - t)\}^2 + (x_2(q) - x_2(p))^2]}{4(\tau - t)} \right] \tag{9}$$

for planar problems. This may also be written as:

$$G(p, \tau; q, t) = \frac{1}{4\pi(\tau - t)} \exp\left[-\frac{r^2}{4(\tau - t)} \right] \exp\left[-\frac{\mathrm{Pe}}{2}(x_1(q) - x_1(p)) \right] \exp\left[-\frac{\mathrm{Pe}^2}{4}(\tau - t) \right] \tag{10}$$

Here, r is the Euclidean distance from the source point to the field point. In (10), the first exponent represents the conduction effects, while the second and third exponents represent the effects due to convection and to transient convection, respectively.

A boundary integral equation for the transient conduction-convection problem may now be obtained by taking the limit as the source point p, inside the domain approaches the point P

on the boundary ($p \to P$). This gives:

$$C(P)T(P,\tau) = \int_0^\tau \mathrm{d}t \int_{\Gamma(t)} \left[G(P,\tau;Q,t)\frac{\partial T}{\partial n_Q}(Q,t) - \frac{\partial G}{\partial n_Q}(P,\tau;Q,t)T(Q,t) \right] \mathrm{d}\Gamma - \mathrm{Pe}\int_0^\tau \mathrm{d}t \int_{\Gamma(t)} G(P,\tau;Q,t)T(Q,t)n_1(Q,t)\,\mathrm{d}\Gamma \tag{11}$$

The coefficient $C(P)$, in general, depends on the local geometry at P. If the boundary is locally smooth at P, $C = 1/2$ for two-dimensional problems. Otherwise, it may be evaluated indirectly[1–3]. In the present work, the coefficient $C(P)$ at a geometric corner is evaluated directly[3] in a Cauchy principal value sense.

NUMERICAL IMPLEMENTATION

Discretization

Numerical implementation of the BEM equations (7), (11) for the transient conduction-convection problem is discussed in this section. The first step is the discretization of the boundary of the two-dimensional domain into boundary elements. In this case, discretizations in both time and space are needed. Accordingly, the boundary is discretized into N spatial boundary elements and the time dimension is subdivided into F time steps. A linear interpolation in space and time is used here for temperature and heat flux:

$$T(\mathbf{x},t) = \sum_{j=1}^{N}\sum_{k=1}^{F} \psi_i \phi^k T_j^k \tag{12}$$

and

$$q(\mathbf{x},t) = \sum_{j=1}^{N}\sum_{k=1}^{F} \psi_i \phi^k q_j^k \tag{13}$$

where ψ and ϕ are interpolation functions in space and time, respectively.

A discretized version of the boundary integral equation (11) may now be written as:

$$\begin{aligned} C(P_M)T(P_M,t_F;Q,t) = {} & \sum_{k=1}^{F}\int_{t_{k-1}}^{t_k} \phi^{k-1}\,\mathrm{d}t \Bigg\{ \sum_{j=1}^{N} \Bigg[\int_{\Delta\Gamma_j(t)} G(P_M,t_F;Q,t)(\psi_j q_j^{k-1} + \psi_{j+1} q_{j+1}^{k-1})\,\mathrm{d}\Gamma_j \\ & - \int_{\Delta\Gamma_j(t)} \frac{\partial G}{\partial n_Q}(P_M,t_F;Q,t)(\psi_j T_j^{k-1} + \psi_{j+1} T_{j+1}^{k-1})\,\mathrm{d}\Gamma_j \\ & - \int_{\Delta\Gamma_j(t)} G(P_M,t_F;Q,t)\mathrm{Pe}\, n_1(Q)(\psi_j T_j^{k-1} + \psi_{j+1} T_{j+1}^{k-1})\mathrm{d}\Gamma_j \Bigg] \Bigg\} \\ & + \sum_{k=1}^{F}\int_{t_{k-1}}^{t_k} \phi^{k}\,\mathrm{d}t \Bigg\{ \sum_{j=1}^{N} \Bigg[\int_{\Delta\Gamma_j(t)} G(P_M,t_F;Q,t)(\psi_j q_j^{k} - \psi_{j+1} q_{j+1}^{k})\,\mathrm{d}\Gamma_j \\ & - \int_{\Delta\Gamma_j(t)} \frac{\partial G}{\partial n_Q}(P_M,t_F;Q,t)(\psi_j T_j^{k} + \psi_{j+1} T_{j+1}^{k})\,\mathrm{d}\Gamma_j \\ & - \int_{\Delta\Gamma_j(t)} G(P_M,t_F;Q,t)\mathrm{Pe}\, n_1(Q)(\psi_j T_j^{k} + \psi_{j+1} T_{j+1}^{k})\,\mathrm{d}\Gamma_j \Bigg] \Bigg\} \end{aligned} \tag{14}$$

In equation (14), $T(P_M)$ represents the temperature at a point P that coincides with node M. T_j^k, T_{j+1}^k, q_j^k, and q_{j+1}^k are nodal values of temperature and flux at time t^k.

Defining ($\gamma = 1, 2$):

$$a_\gamma^k(P_M, \Delta\Gamma_j) = \int_{t_{k-1}}^{t_k} \phi^k \, dt \int_{\Delta\Gamma_j(t_k)} \psi_\gamma \left[\frac{\partial G}{\partial n_Q}(P_M, t_F; Q, t) + \mathrm{Pe}\, n_1(Q) G(P_M, t_F; Q, t) \right] d\Gamma_j \quad (15)$$

and

$$b_\gamma^k(P_M, \Delta\Gamma_j) = \int_{t_{k-1}}^{t_k} \phi^k \, dt_k \int_{\Delta\Gamma_j(t_k)} \psi_\gamma [G(P_M, t_F; Q, t)] \, d\Gamma_j \quad (16)$$

as the coefficient matrices relating the Mth source point with the jth boundary element, we may express (14) in a matrix form:

$$\sum_{k=1}^{F} \sum_{j=1}^{N} [-A_{ij}^{k-1} T_j^{k-1} + B_{ij}^{k-1} q_j^{k-1} - A_{ij}^k T_j^k + B_{ij}^k q_j^k] = 0 \quad (17)$$

Assembled nodal coefficients A_{ij}^k and B_{ij}^k are formed as:

$$A_{ij}^k = a_{(\gamma=2)}^k(i, \Delta\Gamma_{j-1}) + a_{(\gamma=1)}^k(i, \Delta\Gamma_j) + C(i)\Delta(F, k)\Delta(i, j) \quad (18)$$

and

$$B_{ij}^k = b_{(\gamma=2)}^k(i, \Delta\Gamma_{j-1}) + b_{(\gamma=1)}^k(i, \Delta\Gamma_j) \quad (19)$$

Here, $\gamma = 1$ or 2 represents the first or second node of the spatial discretization for the corresponding boundary element. The associated time integration scheme is discussed in detail later.

Integrals of kernels over the elements in (14)–(16) must be obtained carefully. Details of the integration procedure are discussed in a later section.

At each time step and at each location over the entire boundary of the domain, either T or q (or a combination of T and q) is prescribed for a well-posed problem. Also, at each time step, T and q are known at every location on the boundary for all previous time steps. Equation (17) may then be rearranged as:

$$\sum_{j=1}^{N} \tilde{A}_{ij}^F Y_j^F = F_i + \sum_{j=1}^{N} (A_{ij}^{F-1} T_j^{F-1} - B_{ij}^{F-1} q_j^{F-1}) - \sum_{k=1}^{F-1} \sum_{j=1}^{N} (-A_{ij}^{k-1} T_j^{k-1} + B_{ij}^{k-1} q_j^{k-1} - A_{ij}^k T_j^k + B_{ij}^k q_j^k) \quad (20)$$

where F_i is the vector formed by multiplying the known variables by the appropriate coefficient matrix at the final time. Equation (20) may now be used to solve for the unknown variables Y_j^F at the final time.

Integration of kernels in time and space

As observed from equation (10), as t approaches the final time τ, the quantity $(\tau - t)$ approaches zero. This quantity, $(\tau - t)$, appears in the denominator of the expression for $G(P, \tau; Q, t)$ and $\partial G/\partial n_Q(P, \tau; Q, t)$, as well as in the denominator of one of the exponents. So, $G(P, \tau; Q, t)$ or $\partial G/\partial n_Q(P, \tau; Q, t)$ is regular as t approaches τ for $r \neq 0$. However, a singularity occurs if $r \to 0$ at the same time as $t \to \tau$. This is true for the diagonal terms of the G or $\partial G/\partial n_Q$ kernel (when $P \equiv Q$) at the final time.

In the present work, the regular integrands (for all terms when $t < \tau$ and for off-diagonal terms when $t = \tau$) are integrated numerically. The time integrations are performed by a quadrature scheme for improper integrals[19], while the spatial integrations are done by Gauss quadrature.

It is important to note here that the order of the singularity for the diagonal term at the final time is not known *a priori*. In the present work, the term $\exp[-\mathrm{Pe}^2/4(\tau - t)]$ appearing in both G and $\partial G/\partial n_Q$ is first expanded in a Taylor series in $(\tau - t)$. We obtain:

$$G(P, \tau; Q, t) = \frac{1}{4\pi(\tau - t)} \exp\left[-\frac{r^2}{4(\tau - t)}\right] \exp\left[-\frac{\mathrm{Pe}}{2}(x_1(Q) - x_1(P))\right] \times \left[1 + \sum_{n=1}^{\infty} \frac{\left(-\frac{\mathrm{Pe}^2}{4}\right)^n}{n!}(\tau - t)^n\right] \tag{21}$$

and

$$\frac{\partial G}{\partial n_Q}(P, \tau; Q, t) = \frac{-1}{8\pi(t - \tau)^2} \exp\left[-\frac{r^2}{4(\tau - t)}\right] \exp\left[-\frac{\mathrm{Pe}}{2}(x_1(Q) - x_1(P))\right] \times [(x_1(Q) - x_1(P) + Pe(\tau - t))n_1 + (x_2(Q) - x_2(P))n_2] \times \left[1 + \sum_{n=1}^{\infty} \frac{\left(-\frac{Pe^2}{4}\right)^n}{n!}(\tau - t)^n\right] \tag{22}$$

Integrating $\phi^k G(k = F - 1, F)$ in time with $t_k = t_F$, we get:

$$\int_{t_{F-1}}^{t^F} \phi^{F-1} G(P, t_F; Q, t)\, \mathrm{d}t_F = \frac{1}{4\pi\Delta t_F} \exp\left[-\frac{\mathrm{Pe}}{2}(x_1(Q) - x_1(P))\right] \times \left[I_1 + \sum_{n=1}^{\infty} \frac{\left[-\frac{\mathrm{Pe}^2}{4}\right]^n}{n!} I_2\right] \tag{23a}$$

$$\int_{t_{F-1}}^{t^F} \phi^F G(P, t_F; Q, t)\, \mathrm{d}t_F = \frac{1}{4\pi} \exp\left[-\frac{\mathrm{Pe}}{2}(x_1(Q) - x_1(P))\right] \times \left[I_3 + \sum_{n=1}^{\infty} \frac{\left[-\frac{\mathrm{Pe}^2}{4}\right]^n}{n!} I_4\right] - \int_{t_{F-1}}^{t^F} \phi^{F-1} G(P, t_F; Q, t)\, \mathrm{d}t_F \tag{23b}$$

where

$$I_1 = \frac{r^2}{4}\left[\frac{e^{-z_{F-1}}}{z_{F-1}} - E_1(z_{F-1})\right] \tag{23c}$$

with

$$z_{F-1} = \frac{r^2}{4\Delta t_{F-1}} \quad \text{and} \quad E_1(z_{F-1}) = \int_{z_{F-1}}^{\infty} \frac{e^{-\xi}}{\xi}\, \mathrm{d}\xi \tag{23d}$$

Also,

$$I_2 = \left(\frac{r^2}{r}\right)^{n+1}\left[-\sum_{m=1}^{n+1} A^{-1}(m, n+2)(z_{F-1}^{m-(n+2)}\, e^{-z_{F-1}}) + B^{-1}(n+2)E_1(z_{k-1})\right] \tag{23e}$$

with

$$A(m,n)=\prod_{l=1}^{m}[l-n] \qquad \text{and} \qquad B(n)=\prod_{l=1}^{n-1}[l-n] \tag{23f}$$

and

$$I_3=E_1(z_{F-1}) \tag{23g}$$

$$I_4=\left(\frac{r^2}{4}\right)^n\left[-\sum_{m=1}^{n}A^{-1}(m,n+1)(z_{F-1}^{m-(n+1)}e^{-z_{F-1}})+B^{-1}(n+1)E_1(z_{F-1})\right] \tag{23h}$$

It should be noted here that as z_k approaches zero, $E_1(z_k)$ approaches $\ln(z_k)$. Accordingly, the order of singularity in G is of $\ln(r)$ in spatial dimensions and this occurs at the final time.

Similarly, time integration of $\phi^k\,\partial G/\partial n_Q$ gives:

$$\int_{t_{F-1}}^{t^F}\phi^{F-1}\frac{\partial G}{\partial n_Q}(P,t_F;Q,t)\,\mathrm{d}t_F=\frac{\mathrm{d}}{8\pi\Delta t_k}\exp\left[-\frac{\mathrm{Pe}}{2}(x_1(Q)-x_1(P))\right]$$
$$\times\left[I_3+\sum_{n=1}^{\infty}\frac{\left(-\frac{\mathrm{Pe}^2}{4}\right)^n}{n!}I_4\right]-\frac{\mathrm{Pe}\cdot n_1(Q)}{2}\int_{t_{F-1}}^{t_F}\phi^{F-1}G(P,t_F;Q,t)\,\mathrm{d}t_F \tag{24a}$$

$$\int_{t_{F-1}}^{t^F}\phi^{F}\frac{\partial G}{\partial n_Q}(P,t_F;Q,t)\,\mathrm{d}t_F=\frac{\mathrm{d}}{8\pi}\exp\left[-\frac{\mathrm{Pe}}{2}(x_1(Q)-x_1(P))\right]$$
$$\times\left[J_1+\left(-\frac{\mathrm{Pe}^2}{4}\right)I_3+\sum_{n=2}^{\infty}\frac{\left(-\frac{\mathrm{Pe}^2}{4}\right)^n}{n!}J_2\right]$$
$$-\frac{\mathrm{Pe}\cdot n_1(Q)}{8\pi}\exp\left[-\frac{\mathrm{Pe}}{2}(x_1(Q)-x_1(P))\right]\left[I_3+\sum_{n=1}^{\infty}\frac{\left(-\frac{\mathrm{Pe}^2}{4}\right)^n}{n!}I_4\right]$$
$$-\int_{t_{F-1}}^{t^F}\phi^{F-1}\frac{\partial G}{\partial n_Q}(P,t_F;Q,t)\,\mathrm{d}t_F \tag{24b}$$

Here,

$$d=-[(x_i(Q)-x_i(P)]n_i(Q) \qquad \text{when } i=1,2 \tag{24c}$$

$$J_1=\frac{4}{r^2}e^{-z_{F-1}} \tag{24d}$$

$$J_2=\left(\frac{r^2}{4}\right)^{n-1}\left[-\sum_{m=1}^{n-1}A^{-1}(m,n)(z_{F-1}^{m-n}e^{-z_{F-1}})+B^{-1}(n)I_3\right] \tag{24e}$$

Observations of the terms involved in J_1 also reveal that the order of singularity in $\partial G/\partial n_Q$ is $1/r$ in spatial dimensions, and this also occurs at the final time.

After the orders of spatial singularities (at $t=\tau$) in G and $\partial G/\partial n_Q$ are determined, appropriate integration schemes may be used for the diagonal terms at the final time step. Since the kernel

G contains a $\ln r$ singularity, a numerical scheme for integrating improper integrals[22] utilizing Romberg integration as an open interval is used for spatial integration of the singular terms of G. The kernel $\partial G/\partial n_Q$, however, contains stronger singularities of order $1/r$. The diagonal terms of $\partial G/\partial n_Q$ integrated analytically using published methods.[1-3]

NUMERICAL RESULTS

Figure 1 shows a schematic diagram of the test problem. The boundary conditions are:

$$T = 1, \quad x_1 = 0, \quad 0 \leqslant x_2 \leqslant 1 \tag{25a}$$

$$T = 0, \quad x_1 = 1, \quad 0 \leqslant x_2 \leqslant 1 \tag{25b}$$

$$q = 0, \quad x_2 = 0, \quad 0 \leqslant x_1 \leqslant 1 \tag{25c}$$

$$q = 0, \quad x_2 = 1, \quad 0 \leqslant x_1 \leqslant 1 \tag{25d}$$

and the initial condition is:

$$T = 0, \qquad t = 0 \tag{25e}$$

The boundary conditions specified above represent a one-dimensional problem. A closed-form analytical solution is obtained using the method of separation of variables. This may be expressed as:

$$T(\mathrm{x}, t) = 2 \sum_{n=1}^{\infty} \frac{n\pi}{\lambda_n} \{1 - \exp(-\lambda_n t)\} \exp\left(\frac{(\mathrm{Pe})\mathrm{x}}{2}\right) \sin(n\pi x) \tag{26}$$

where

$$\lambda_n = \left(\frac{\mathrm{Pe}}{2}\right)^2 + (n\pi)^2$$

A standard successive-over-relaxation finite difference method (SOR) is also used to solve (2) subject to boundary and initial conditions in (25a–e). In this finite difference solution, the conduction term is approximated by a central difference, the convective term is modelled by an upwind difference, and the transient part is modelled by the Crank–Nicolson technique.

Figure 2 shows the transient fields for Pe = 20 for five different times. The BEM results are obtained using a uniform mesh size of 0.1 and a constant time increment of 0.01. The SOR

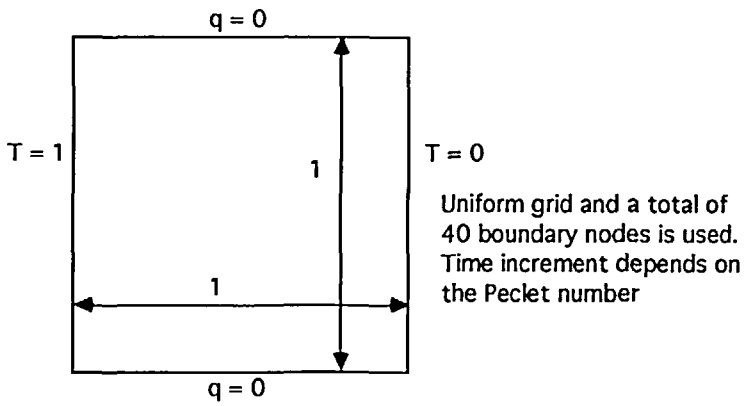

Figure 1 Schematic diagram of the test problem (uniform grid and a total of 40 nodes are used; time increment depends on the Peclet number)

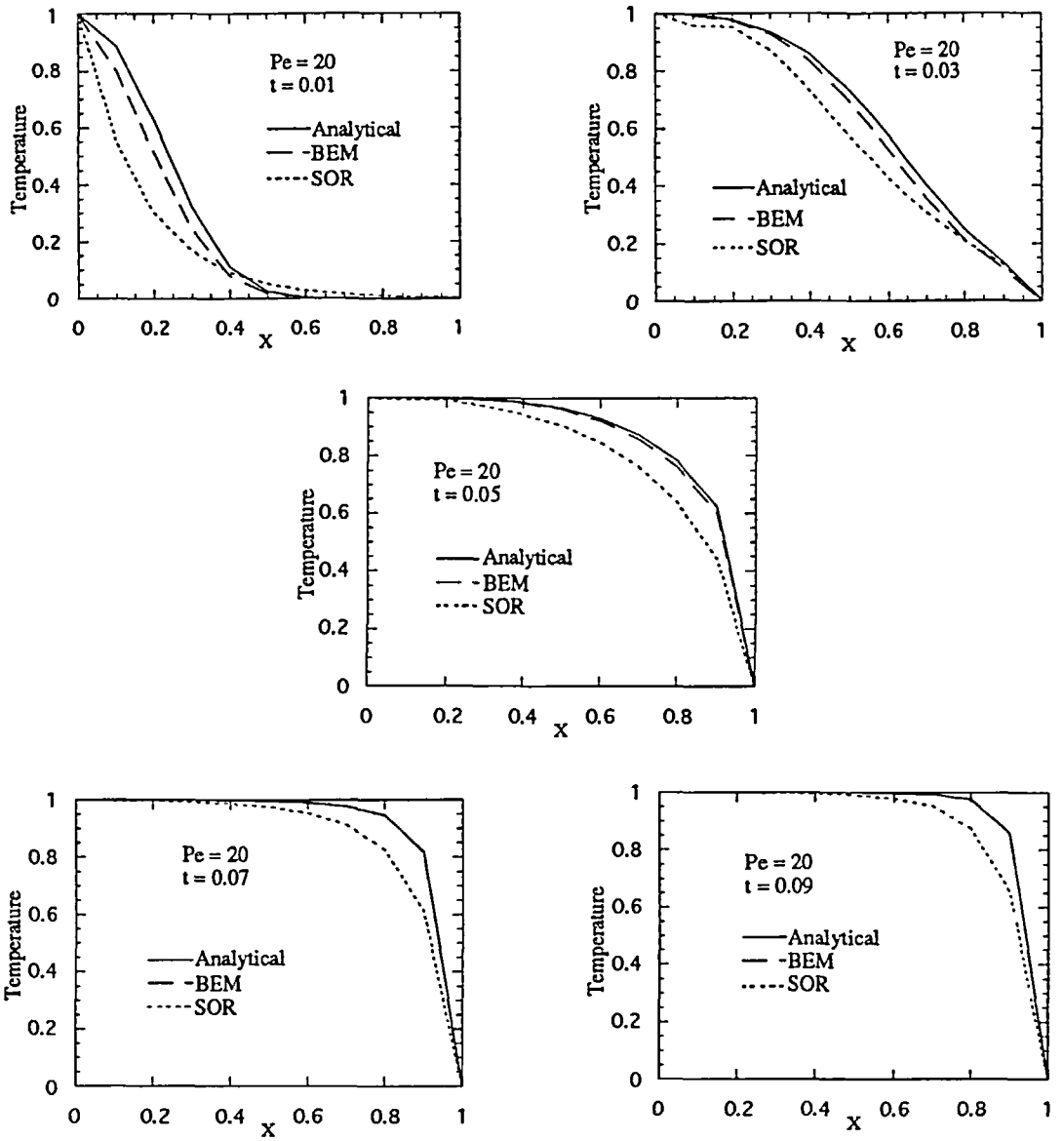

Figure 2 Comparison of the BEM solution with the analytical and SOR solutions at Pe = 20 and $\Delta x = 0.1$

results were obtained using the same uniform mesh size and time increment. It can be observed that the BEM results closely match the analytical results. Further, the BEM performs much better in predicting the temperature profiles. In SOR, the false diffusion caused by the upwind difference of the convective term introduces large errors in the temperature field. The results from SOR using a uniform mesh size of 0.01 and time increment of $\Delta t = 10^{-4}$ are plotted in *Figure 3*. It is clear that the SOR results can be improved by reducing the grid size. However, the computation time required to obtain these fine-mesh results is considerably longer because of the decrease in Δx and Δt. Moreover, these refinements make the computational time prohibitively large for higher Peclet numbers. In the BEM formulation, the Green's function

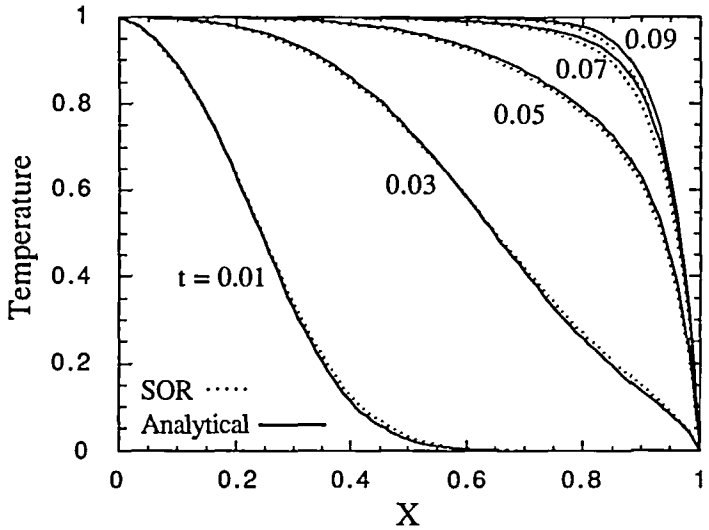

Figure 3 Comparison of the SOR solution with the analytical solution at Pe = 20, $\Delta x = 0.01$, $t = 0.01$–0.09 by 0.02, and $\Delta t = 10^{-5}$

used is the transient moving heat source solution[21] which gives a better approximation of the convective term. Consequently, false diffusion is minimized[15,17].

As the Peclet number increases, the problem becomes convection dominated. The simple Galerkin formulation in FEM produces an unstable solution. The Petrov–Galerkin method[1] for steady-state problems does obtain a stable solution. Yu and Heinrich[8] extended the Petrov–Galerkin formulation to a transient convection transport equation. The Petrov–Galerkin formulation produces a stable solution, however, the discrepancy in maximum temperature with the analytical solution is noticeable.

To illustrate the capability of the BEM formulation in handling high Peclet number convection, the transient fields for Pe = 2000 for five different times are plotted in *Figure 4*. The results were obtained for a uniform mesh size of 0.1 and a constant time increment of 10^{-5} for the BEM calculation and a uniform mesh size of 0.01 and a constant time increment of 10^{-5} for the SOR calculation. It can be observed that there is a very good match between the BEM results and those of the asymptotic solutions. The analytical solution given in (26) fails to converge for Pe = 2000. Consequently, we have tried to compare it with the asymptotic solution. The detailed derivation of the asymptotic solution is given in the Appendix. In the limit of large Pe numbers, the convection term dominates and the problem can be solved using asymptotic expansion. The outer region is dominated by convection, whose solution is a sharp temperature front moving downstream with the wave velocity. Around the wave front, the inner region, scaled like $\mathrm{Pe}^{-1/2}$, is dominated by diffusion. The solution can be expressed as:

$$T(x_1, t) = \begin{cases} \dfrac{1}{2}\left[2 - \operatorname{erfc}\left(-\dfrac{(x_1 - t)\mathrm{Pe}}{2t^{1/2}}\right)\right], & x_1 \leqslant \mathrm{Pe} \\ \dfrac{1}{2}\operatorname{erfc}\left(\dfrac{(x_1 - t)\mathrm{Pe}}{2t^{1/2}}\right), & x_1 > \mathrm{Pe} \end{cases} \tag{27}$$

Figure 4 shows that the phenomenon is accurately captured by the BEM; however, the SOR is totally inadequate. It should be pointed out that the time increment was reduced from 10^{-2} (Pe = 20) to 10^{-5} (Pe = 2000) in the BEM calculations. The BEM formulation is unconditionally

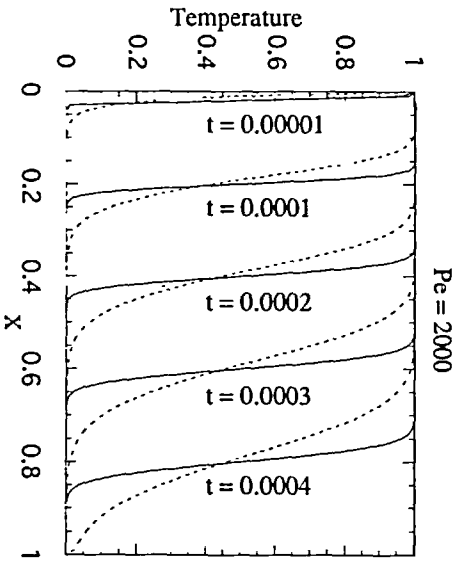

Figure 4 Comparison of the BEM solution with the asymptotic and SOR solutions at Pe = 2000 and $\Delta x = 0.01$ (dashed lines = SOR results; solid lines = BEM and analytical results)

Table 1 Relationship between Δt and maximum *Pe*'s

	BEM		SOR	
Δt	Maximum *Pe*	ΔX	Maximum *Pe*	ΔX
1×10^{-2}	100	0.1	10	0.1
1×10^{-3}	300	0.1	30	0.03
1×10^{-4}	1,000	0.1	100	0.01
1×10^{-5}	2,100	0.1	300	0.003

stable. It was observed that the term $(\mathrm{Pe}^2/4)^n(\tau - t)^n$ in (21) and (22) has a tendency to create an overflow in the computer for high Peclet numbers. This may be avoided by choosing a time increment so that the above term is less than the overflow capacity of the computer. *Table 1* shows the maximum Peclet numbers for a fixed time increment. The table was generated by fixing the time increment and increasing the Peclet number until the program terminated with an overflow error message. Double precision was used in these calculations. In the case of SOR, the time increment is limited by the stability criterion of the Courant number being less than 1^{23}. The Courant number may be defined as $\mathrm{Pe}(\Delta t/\Delta x)$. As Pe increases, the grid size has to be decreased to capture the high gradients. This can be observed from the results of Pe = 20 given in *Figures 2* and *3*. In order to capture the steep gradient, the grid size should be 0.01 and the time increment reduced to 10^{-4}. As a result, the time increment should be restricted to $\Delta t \sim \mathrm{Pe}^{-2}$.

In order to compare the accuracies of the BEM and SOR methods, we define the following errors. The error at each time step is defined as:

$$E = \sqrt{\sum_{i=1}^{n} \frac{(T - T_i)^2}{N}} \tag{28}$$

Table 2 RMS error of BEM and SOR results

		RMS error	
Pe	*t*	BEM	SOR
1.0	0.01	4.77801×10^{-2}	7.78740×10^{-2}
	0.03	1.38802×10^{-2}	2.08699×10^{-2}
	0.05	9.01710×10^{-3}	1.14195×10^{-2}
	0.07	7.04800×10^{-3}	7.01487×10^{-3}
	0.09	5.77009×10^{-3}	4.44575×10^{-3}
5.0	0.01	5.28524×10^{-2}	8.86331×10^{-2}
	0.03	1.90902×10^{-2}	1.92125×10^{-2}
	0.05	1.42936×10^{-2}	1.04627×10^{-2}
	0.07	1.17259×10^{-2}	8.56085×10^{-3}
	0.09	9.41962×10^{-3}	8.38559×10^{-3}
10.0	0.01	5.66623×10^{-2}	0.109351
	0.03	2.52636×10^{-2}	3.55529×10^{-2}
	0.05	1.97946×10^{-2}	2.92629×10^{-2}
	0.07	1.39803×10^{-2}	3.64733×10^{-2}
	0.09	8.56032×10^{-3}	4.92900×10^{-2}
20.0	0.01	5.51768×10^{-2}	0.164496
	0.03	3.23170×10^{-2}	9.54526×10^{-2}
	0.05	1.44366×10^{-2}	9.56546×10^{-2}
	0.07	3.44543×10^{-3}	8.66238×10^{-2}
	0.09	1.55643×10^{-3}	7.89693×10^{-2}

where T is the analytical solution, T_i is the approximate solution, and N is the number of nodes. The errors of the centerline temperature ($y = 0.5$) for both BEM and SOR results are tabulated in *Table 2*. It can be observed that, for the same mesh size, BEM results have smaller errors than the SOR, except for the case of Pe = 5.0. In an attempt to determine the reason, temperature fields at various time steps were plotted, *Figure 5*. It can be observed that the SOR prediction gives a lower temperature at the beginning of the domain and a higher temperature at the end, resulting in a smaller error (28).

CONCLUSIONS

A boundary element method (BEM) formulation for two-dimensional transient conduction-convection problems is developed in this paper. The BEM formulation is based on the time-dependent fundamental solution of the transient conduction-convection operator. Thus, the governing parabolic partial differential equation is reduced to a boundary-only form that does not require any domain discretization. This makes the proposed algorithm stable and avoids any false diffusion. Irregular boundaries may be easily handled by the BEM. The boundary-only formulation also requires a small amount of core memory.

The two-dimensional BEM algorithm is applied to solve a one-dimensional problem whose analytical solution is possible by separation of variables. A standard successive-over-relaxation finite difference method (SOR) is also applied to the same problem. All of these results are compared to each other. The asymptotic solution for large Pe, where the method of separation of variables fails, is also obtained and compared to BEM and SOR results. It is found that the BEM provides a more accurate solution than SOR for the same mesh size. This implies that the SOR will require a finer mesh size for the same degree of accuracy.

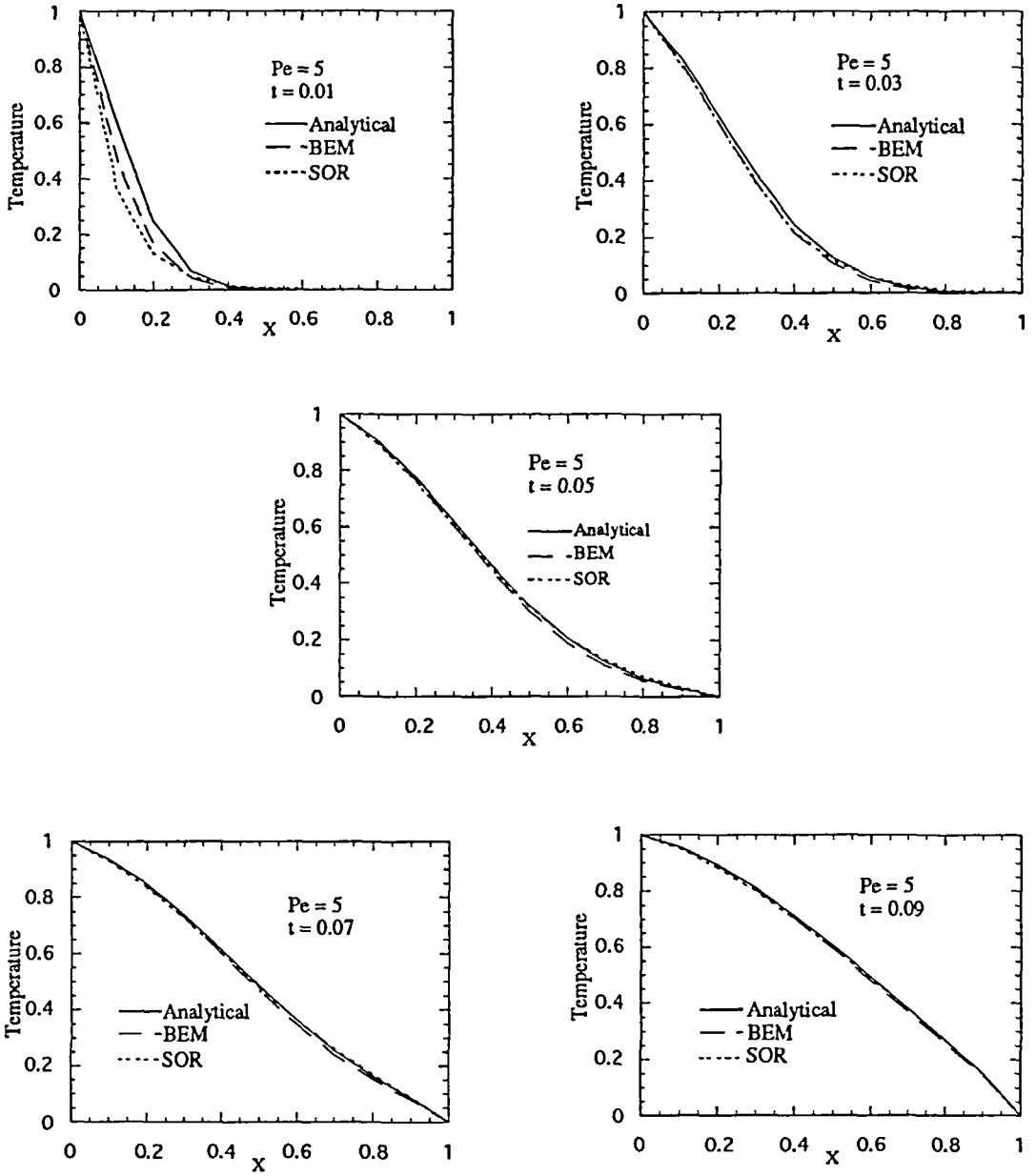

Figure 5 Comparison of the BEM solution with the analytical and SOR solutions at Pe = 5 and $\Delta x = 0.1$

ACKNOWLEDGEMENTS

The authors gratefully acknowledge the financial support provided by the US National Science Foundation under Grants CTS-8909101 and DMC-8657345 and the support received from the Hughes Aircraft Company.

APPENDIX: ASYMPTOTIC SOLUTION IN THE LIMIT OF LARGE PECLET NUMBERS

The one-dimensional form of governing equation (2) can be expressed as:

$$\frac{\partial T(x_1,t)}{\partial t} + \mathrm{Pe}\frac{\partial T(x_1,t)}{\partial x_1} = \frac{\partial^2 T(x_1,t)}{\partial x_1^2} \tag{A1}$$

The initial boundary conditions are:

$$t = 0, \quad T = 0 \tag{A2}$$

$$t > 0, \quad x = 0, \quad T = 1 \tag{A3}$$

$$t > 0, \quad x = 1, \quad T = 0 \tag{A4}$$

It is more convenient to express the equation in the dimensionless form using the convective time scale:

$$t^* = t\,\mathrm{Pe} \tag{A5}$$

The governing equation becomes:

$$\frac{\partial T(x_1,t^*)}{\partial t^*} + \frac{\partial T(x_1,t^*)}{\partial x_1} = \frac{1}{\mathrm{Pe}}\frac{\partial^2 T(x_1,t^*)}{\partial x_1^2} \tag{A6}$$

In the limit of large Pe numbers, the outer region is governed by the one-dimensional wave equation:

$$\frac{\partial T^\circ(x_1,t^*)}{\partial t^*} + \frac{\partial T^\circ(x_1,t^*)}{\partial x_1} = 0 \tag{A7}$$

subject to the initial and boundary conditions:

$$t^* = 0, \quad T^\circ = 0 \tag{A8}$$

$$t^* > 0, \quad x_1 = 0, \quad T^\circ = 1 \tag{A9}$$

The solution is a temperature front:

$$T^\circ(x_1,t) = \begin{cases} 1, & x_1 \leqslant t^* \\ 0, & x_1 > t^* \end{cases} \tag{A10}$$

We now focus on the inner region. Introduce the inner variables:

$$\eta = (x_1 - t^*)\,\mathrm{Pe}^{1/2} \tag{A11}$$

The zeroeth order is governed by:

$$\frac{\partial T^i}{\partial t^*} = \frac{\partial^2 T^i}{\partial \eta^2} \tag{A12}$$

The initial and boundary conditions are:

$$t^* = 0, \quad T^i = \begin{cases} 1, & \eta \leqslant 0 \\ 0, & \eta > 0 \end{cases} \tag{A13}$$

$$t^* > 0, \quad T^i = 1 \quad \text{as } \eta \to -\infty \tag{A14}$$

$$t^* > 0, \quad T^i = 0 \quad \text{as } \eta \to \infty \tag{A15}$$

The matching conditions are incorporated in equations (A14), (A15). In the original independent variables, the solution can be expressed as:

$$T(x_1, t) = \begin{cases} \frac{1}{2}\left[2 - \operatorname{erfc}\left(-\frac{(x_1 - t)\,\mathrm{Pe}}{2t^{1/2}}\right)\right], & x_1 \leqslant \mathrm{Pe} \\ \frac{1}{2}\operatorname{erfc}\left(\frac{(x_1 - t)\,\mathrm{Pe}}{2t^{1/2}}\right), & x_1 > \mathrm{Pe} \end{cases} \tag{A16}$$

This inner solution is in fact valid for the entire region, provided that Pe is large.

REFERENCES

1 Banerjee, P. K. and Butterfield, R. *Boundary Element Methods in Engineering Science*, McGraw-Hill, London (1981)
2 Mukherjee, S. *Boundary Element Methods in Creep and Fracture*, Elsevier Applied Science Pub. (1982)
3 Brebbia, C. A., Telles, J. C. F. and Wrobel, L. C. *Boundary Element Techniques—Theory and Applications in Engineering*, Springer-Verlag, Berlin (1984)
4 Beskos, D. E. (Ed.) *Boundary Element Methods in Mechanics*, North-Holland, Amsterdam (1987)
5 Mukherjee, S. and Morjaria, M. On the efficiency and accuracy of the boundary element method and finite element method, *Int. J. Num. Meth. Eng.*, **20**, 515–522 (1982)
6 Christies, I., Griffiths, D. F., Mitchell, A. R. and Zienkiewicz, O. C. Finite element methods for second order differential equations with significant first derivatives, *Int. J. Num. Meth. Eng.*, **10**, 1389–1396 (1976)
7 Zienkiewicz, O. C., Gallagher, R. H. and Hood, P. Newtonian and non-Newtonian viscous incompressible flow. Temperature induced flows. Finite element solution. *2nd Conference, Mathematics of Finite Elements and Applications*, Academic Press (1976)
8 Yu, C.-C. and Heinrich, J. C. Petrov-Galerkin methods for the time-dependent convective transport equation, *Int. J. Num. Meth. Eng.*, **23**, 883–901 (1986)
9 Rizzo, F. J. and Shippy, D. J. A method of solution for certain problems of transient heat condcution, *AIAA J.*, **9**, 2004–2009 (1970)
10 Curran, D. A. S., Lewis, B. A. and Cross, M. A boundary element method for the solutions of the transient diffusion equation in two dimensions, *Appl. Math. Modelling*, **10**, 107–113 (1986)
11 Fleuries, J. and Predeleanu, M. On the use of coupled fundamental solutions in BEM for thermoelastic problems, *Eng. Analysis*, **4**, 70–74 (1987)
12 O'Neill, K. Boundary integral equation solution of moving boundary phase change problems, *Int. J. Num. Meth. Eng.*, **19**, 1825–1850 (1983)
13 Zabaras, N. and Mukherjee, S. An analysis of solidification problems by the boundary element method, *Int. J. Num. Meth. Eng.*, **24**, 1879–1900 (1987)
14 Aral, M. M. and Tang, Y. A boundary-only procedure for transient transport problems with or without first order chemical reactions, *Appl. Math. Modelling*, **13**, 130–137 (1989)
15 Tanaka, Y., Honma, T. and Kaji, I. On mixed element solutions of convection-diffusion problems in three dimensions, *Appl. Math. Modelling*, **10**, 170–175 (1986)
16 Chan, C. L. and Chandra, A. An algorithm for handling corners in the boundary element method: applications to conduction-convection equations, *Appl. Math. Modelling*, **15**, 244–255 (1991a)
17 Chan, C. L. and Chandra, A. A boundary element method analysis of the thermal aspects of metal cutting processes, *ASME J. Eng. Ind.*, **113**, 311–319 (1991b)
18 Chan, C. L. and Chandra, A. Thermal aspects of machining processes and their design sensitivities: a BEM approach, *Appl. Math. Modelling*, **15**, 562–575 (1991c)
19 Chandra, A. and Chan, C. L. A BEM formulation for design sensitivities in steady-state conduction-convection problems, *ASME J. Appl. Mech.*, **59**, 182–190 (1992)
20 Curran, D. A. S., Cross, M. and Lewis, B. A. Solution of parabolic partial differential equations by the boundary element method using discretization in time, *Appl. Math. Modelling*, **4**, 398–400 (1980)
21 Carslaw, H. S. and Jaeger, J. C. *Conduction of Heat in Solids*, 2nd Ed., Clarendon Press, Oxford (1986)
22 Press, W. H., Flannery, B. P., Tenkolsky, S. A. and Vetterling, W. T. *Numerical Recipes*, Cambridge University Press (1986)
23 Anderson, D. A., Tannehill, J. C. and Pletcher, R. H. *Computational Fluid Mechanics and Heat Transfer*, New York: Hemisphere Publishing Corp. (1989)